APPLIED PHYSICS LETTERS **105**, 032103 (2014)

Intermediate band conduction in femtosecond-laser hyperdoped silicon

Meng-Ju Sher[1,a)] and Eric Mazur[1,2]
[1]Department of Physics, Harvard University, 9 Oxford Street, Cambridge, Massachusetts 02138, USA
[2]School of Engineering and Applied Sciences, Harvard University, 9 Oxford Street, Cambridge, Massachusetts 02138, USA

(Received 4 April 2014; accepted 8 July 2014; published online 23 July 2014)

We use femtosecond-laser hyperdoping to introduce non-equilibrium concentrations of sulfur into silicon and study the nature of the resulting intermediate band. With increasing dopant concentration, the sub-bandgap absorption increases. To better understand the dopant energetics, we perform temperature-dependent Hall and resistivity measurements. We analyze the carrier concentration and the energetics of the intermediate band using a two-band model. The temperature-dependence of the carrier concentration and resistivity suggests that the dopant concentration is below the insulator-to-metal transition and that the samples have a localized intermediate band at 70 meV below the conduction band edge. © *2014 AIP Publishing LLC*. [http://dx.doi.org/10.1063/1.4890618]

In recent years, advances in doping techniques have made it possible to achieve non-equilibrium concentrations of dopants in host materials. Beyond traditional choices of dopants, hyperdoping silicon with deep-level chalcogen dopants (S, Se, or Te) changes the optical,[1,2] electronic,[3] and optoelectronic properties[4–6] of Si. These unusual properties result from the high dopant concentration, which broadens a dopant energy level into a band,[7] often referred to as an impurity or intermediate band (IB).[8] To develop applications of deep-level intermediate-band materials, knowledge of the intermediate band energetics is essential. In this work, we report the electronic transport properties of Si supersaturated with S dopants and present methods to identify the energetic of the intermediate band.

The formation and properties of impurity bands have been studied in many host materials with shallow dopants.[9–11] At a critical concentration, n_{crit}, electron-electron interaction leads to a delocalized dopant energy band instead of a single dopant energy level. Charge carriers can freely conduct in this delocalized impurity band, giving rise to a finite conductivity even at temperatures near absolute zero, and hence the transition to a delocalized energy band is often referred to as an insulator-to-metal transition. For samples with dopant concentrations just below n_{crit}, experiments show that these samples exhibit low-temperature conductivity due to carrier hopping.[12,13] The electron wave functions are localized, but the temperature dependence of the carrier concentration does not exhibit any freeze out of carriers from a single dopant energy level. In order to describe the observed temperature dependence of the electronic transport data at concentrations near n_{crit}, a two-band model takes both the conduction band (CB) and an IB into account.[14,15]

It has been suggested that the efficiency of photovoltaic cells could be improved by using a deep IB,[16] but fabricating such a band poses a significant challenge. Because of the low solid solubility of deep level dopants,[17] reliable hyperdoping techniques are required to incorporate high concentrations of deep level dopants. Examples of deep level dopants include heavy chalcogens.[18] High concentrations of chalcogen dopants in Si have been achieved through ion implantation, and several studies have reported low temperature conductivity of the resulting samples but it is hard to rule out implantation damage as a cause of this conductivity.[19–21] Winkler *et al.* used ion-implantation followed by nanosecond-pulsed laser melting to heal the crystal lattice of S-hyperdoped Si and observed an insulator-to-metal transition between 1.8 and $4.3 \times 10^{20}\,\mathrm{cm}^{-3}$.[3] In addition to determining n_{crit}, understanding the properties of deep-level impurity bands remains an active area of research.[6,7,22–25]

In this paper, we use femtosecond-laser hyperdoping[26] to introduce non-equilibrium concentrations of S into Si and report evidence for a localized band formation below the insulator-to-metal transition. This paper provides analysis techniques to study deep level hyperdoped systems. We present methods to study the low-temperature electronic transport data and identify the location of the IB. As a deep-level IB is desired for applications such as intermediate-band photovoltaics,[16] these findings are important for evaluating S-hyperdoped Si for potential photovoltaic applications.

Si wafers (p-type, 10 Ω cm, (100) orientation) are cleaned to remove organic and metallic contaminants.[27] The wafers are placed in a chamber and irradiated at normal incidence with Ti:sapphire laser pulses (80-fs pulse duration, 800-nm center wavelength, and 1-kHz repetition rate). The chamber is filled with sulfur hexafluoride (SF_6) gas at a pressure between 0.13 and 13.0 kPa. The laser pulses have an average energy of 1.0 mJ and are focused to a spot size of 600 μm (FWHM of Gaussian intensity profile), yielding a fluence of 2.5 kJ/m^2. A set of scanning mirrors scans the laser beam and translates subsequent pulses by 75 μm such that any given spot in the irradiated region is exposed to 50 laser pulses. After laser irradiation, samples are annealed at 975 K for 30 min. in an open-tube furnace with a 300-sccm flow of forming gas (95% He, 5% H_2). The fabrication process causes surface texturing, which enhances the absorptance of the sample.[28] Using a spectrophotometer equipped with an integrating sphere, we collect transmission (T_{int}) and reflection (R_{int}) spectra and determine the absorptance ($A = 1 - R_{int} - T_{int}$). We use secondary ion mass

a)Email: msher@stanford.edu

 © 2014 AIP Publishing LLC

This article is copyrighted as indicated in the article. Reuse of AIP content is subject to the terms at: http://scitation.aip.org/termsconditions.

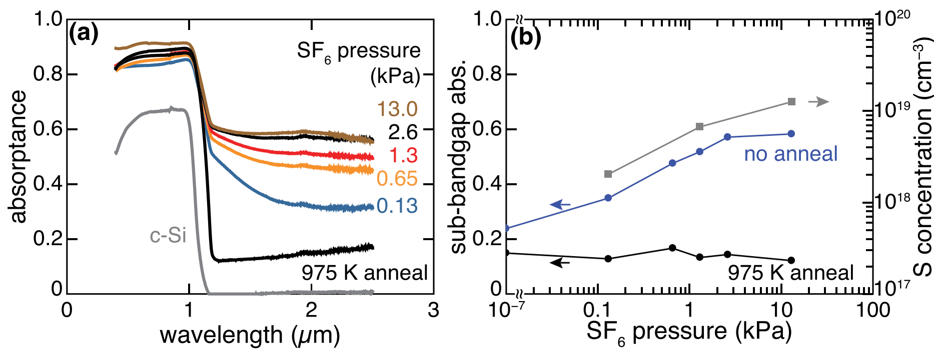

FIG. 1. (a) Absorptance of S-hyperdoped Si before and after annealing. After annealing, the sub-bandgap absorptance between different samples are the same, so for clarity, only one curve is shown. (b) Average sub-bandgap absorptance and sulfur concentration of samples hyperdoped at different pressures of SF_6.

spectrometry (SIMS) measurements to determine the sulfur concentrations in the samples.

To determine the electronic properties of the samples, we cut them into 6-mm squares and deposit 1.2-mm square Ti-Ni-Ag contacts (20–20–200 nm, with the Ti contacting the Si) at four corners of the samples. We also deposit Al contacts at the back of the samples for measuring the current-voltage properties of the junction between the laser-doped region and the substrate. We focus here only on the samples annealed at 975 K, because we find that only the samples annealed at 975 K or higher temperatures exhibit diode formation between the hyperdoped region and the substrate. A rectifying junction between the hyperdoped layer (n-type) and the substrate (p-type) isolates the measurement current to within the hyperdoped layer and allow us to probe only the properties of the hyperdoped layer. We use the van der Pauw technique for temperature-dependent resistivity and Hall measurements.[29] To avoid self-heating effects and minimize measurement errors, we use a constant excitation power between 25 and 100 nW. Measurement temperatures between 10 and 300 K are controlled by a closed-cycle helium cryostat. All Hall measurements are performed at a magnetic field $B = 0.6$ T.

We obtain the sheet carrier concentration n_s from the measured Hall voltage V_H using the relationship $n_s = r_H IB/(qV_H)$, where r_H is the Hall scattering factor, I is the excitation current, and q is the elementary charge. If the hyperdoped layer thickness d is well defined, the carrier concentration is $n_H = n_s/d$. In this work, we focus our analysis on the temperature dependence of n_s and we normalize n_s to the value measured at 300 K. This normalization allows us to avoid the uncertainty associated with the thickness d and the Hall scattering factor r_H.

Figure 1(a) shows the average sub-bandgap light absorptance of samples hyperdoped at different SF_6 pressures. The data show that the sub-bandgap absorption increases with increasing SF_6 pressure. Annealing decreases the sub-bandgap light absorption, however, and the post-anneal absorptance no longer depends on SF_6 pressure. This residual sub-bandgap light absorption of 0.2 could be due to light scattering out of the integrating sphere. Figure 1(b) shows the average sub-bandgap absorption and the S dopant concentration. Because of the rough sample surface, the SIMS measurement does not have depth resolution and we report data averaged over a depth range from 100 to 500 nm. The SIMS measurements indicate that the S concentration increases with pressure from 2.0×10^{18} to $1.3 \times 10^{19}\,\mathrm{cm}^{-3}$. After annealing at 975 K, the SIMS measurements reveal no difference in S concentration (Table I).

Figure 2 shows the sheet carrier concentration and sheet resistivity as a function of inverse temperature. The Hall measurement data indicate n-type carriers for all four samples over the entire temperature range. Figure 2(a) shows that the carrier concentration exhibits little temperature dependence. In contrast, the carriers in the p-type Si substrate freeze out quickly as the sample cools down. Fitting the carrier concentration for the p-type substrate when they freeze out at temperatures between 25 and 82 K, we obtain a value of 48 ± 3 meV for the boron dopant energy level, in good agreement with the literature value (45 meV).[30] To further investigate the temperature-dependent carrier concentrations, the inset of Figure 2(a) shows normalized sheet carrier concentration. We observe a systematic increase of the normalized carrier at low temperature with respect to room temperature. Notably, samples C and D have a greater carrier concentration at low temperature than at room temperature.

Let us now discuss the nature of the IB and present a model to describe transport properties of hyperdoped Si. Figure 2(a) shows that the carrier concentration in the hyperdoped sample does not freeze out as the temperature decreases, suggesting the formation of an IB where electrons can conduct at low temperatures. At the same time, because the resistivity increases as temperature decreases (Figure 2(b)), the samples do not exhibit a metallic-like conduction so the electron wave function in the IB is not fully delocalized. In other words, the dopant concentration in our samples is below n_{crit}, but the transport measurements show band-like behavior. To analyze the energetics of the dopant electrons we present a two-band (CB and IB) model, taking into account carrier conduction in both bands.

Figure 3(a) shows a schematic of the two-band model, with the IB isolated from the CB. If the carriers in the IB are mobile, they contribute to the transport measurement. We

TABLE I. Sulfur concentrations and two-band model fitting results for samples hyperdoped at different SF_6 pressures.

Sample	SF_6 pressure (kPa)	SIMS S concentration ($10^{18}\,\mathrm{cm}^{-3}$)	Two-band model N_d ($10^{18}\,\mathrm{cm}^{-3}$)	Two-band model ΔE (meV)	Two-band model b
A	0.13	2.0 ± 0.3	…	…	…
B	1.3	6.7 ± 1.0	0.002	150 ± 60	4.4
C	2.6	…	0.4 ± 0.2	80 ± 10	4.7
D	13.0	13 ± 2	1.1 ± 0.6	70 ± 10	6.4
D no ann	13.0	16 ± 2	…	…	…

This article is copyrighted as indicated in the article. Reuse of AIP content is subject to the terms at: http://scitation.aip.org/termsconditions.

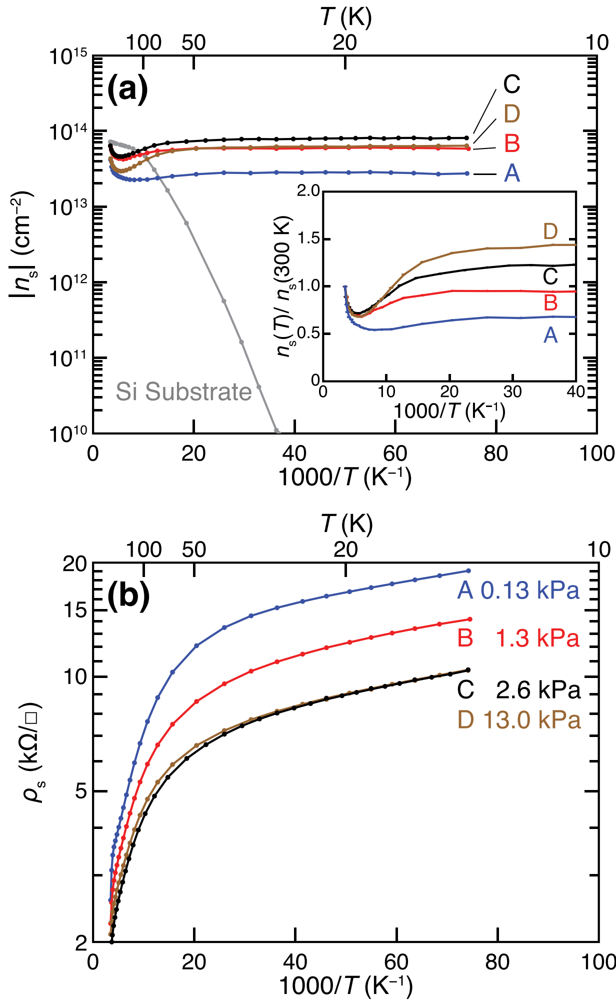

FIG. 2. Temperature-dependent transport measurements: (a) sheet carrier concentration, and (b) sheet resistivity. Samples A, B, C, and D refer, respectively, to Si hyperdoped at different SF_6 pressures and followed by a 30-min annealing at 975 K. Sheet carrier concentration data for the Si substrate (p-type) are shown for comparison. Normalized carrier concentration is shown as an inset in (a).

denote the energy gap between the two bands by ΔE, and the mobilities of the carriers in the CB and IB by μ_c and μ_i, respectively. The concentration of carriers in the CB and IB are n_c and n_i, respectively. We use subscripts c, i, and, H to denote properties of the CB, the IB, and the transport measurements, respectively. The measured conductivity σ_H is the sum of the contribution to the conductivity from each of the two bands, $\sigma_H = \sigma_c + \sigma_i = e\,(n_c\,\mu_c + n_i\,\mu_i)$. The measured Hall carrier concentration, n_H, is given by[14]

$$\frac{1}{n_H} = \left(\frac{\sigma_c}{\sigma_H}\right)^2 \frac{1}{n_c} + \left(\frac{\sigma_i}{\sigma_H}\right)^2 \frac{1}{n_i}. \tag{1}$$

At high temperature, most carriers are excited into the CB, so n_H is approximately equal to n_c, and the measured carrier concentration is just due to the carriers in the CB. At low temperature, all the carriers are in the ground state, so n_H is approximately n_i. At intermediate temperatures, Eq. (1) implies that n_H exhibits a minimum. Figure 2(a) shows the characteristic shape of the n_H curve as a function of inverse temperature: a minimum dip followed by a temperature-independent line at lower temperatures.[13] To simplify Eq. (1), we define $b = \mu_c/\mu_i$ and $x = n_i/n_c$. This yields

$$n_H = n_c\,\frac{(b+x)^2}{b^2+x}. \tag{2}$$

Emelyanenko *et al.* assume that b depends much more weakly on temperature than x, so b can be approximated as a constant in Eq. (2).[14] With that approximation, it is straightforward to describe the transport data with semiconductor statistics.

To calculate n_H we assume the width of the IB to be small compared to ΔE and,[14] because our experiment focuses on the transport properties at low temperature, we approximate the material as a single donor system.[31] With these simplifications, the concentration of carriers in the IB is given by $n_i = \frac{N_d}{1+\frac{1}{2}e^{(E_d-E_f)/(kT)}}$, where N_d, E_d, and E_f are the donor concentration, dopant energy level, and the Fermi level, respectively; T is the temperature, k is the Boltzmann's constant, and the factor 1/2 in the denominator indicates the band is localized.[11] Furthermore, we assume our material system is in a non-degenerate regime and solve n_c using both Fermi statistics, $n_c = N_c e^{(E_f-E_c)/(kT)}$, and conservation of charge carriers, $n_c = N_d - N_a - n_i$, where N_c is the effective density of states in the CB, and N_a is the concentration of compensating acceptors.[32] The solution for n_c is $\frac{1}{2}\left(-N_a - \frac{N_c}{2}e^{-\Delta E/(kT)} + \sqrt{\left(N_a - \frac{N_c}{2}e^{-\Delta E/(kT)}\right)^2 + 2N_dN_ce^{-\Delta E/(kT)}}\right)$ and for n_i is $N_d - N_a - n_c$. Finally, with b constant, we can calculate n_H

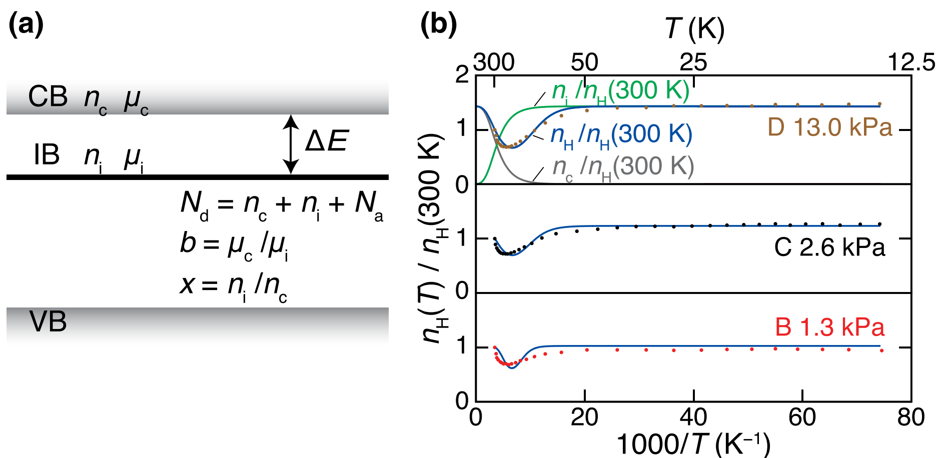

FIG. 3. (a) Two-band model schematics. (b) Normalized carrier concentrations of sample B, C, D, and fitted curves. Measured data are shown in dots; blue solid lines are fitting results. For Sample D, values of n_i (green) and n_c (gray) are also shown.

This article is copyrighted as indicated in the article. Reuse of AIP content is subject to the terms at: http://scitation.aip.org/termsconditions.

using Eq. (2) and fit our data using N_d, ΔE, and b as adjustable parameters.

We performed a least-squares fit of the normalized data shown in the inset of Figure 2(a). As stated earlier, normalizing the data eliminates the sample thickness d from the analysis and so $n_s(T)/n_s(300\,\mathrm{K}) = n_H(T)/n_H(300\,\mathrm{K})$. The quality of the fit depends only weakly on N_a, and so we excluded N_a from the fitting routine ($N_a = 0$). Figure 3(b) shows the resulting fits and Table I gives the fitting parameters. For sample D, we also plot n_i and n_c to show the distribution of carriers in the two bands. Table I shows that N_d ($10^{18}\,\mathrm{cm}^{-3}$) is much smaller than n_crit for Si:S ($10^{20}\,\mathrm{cm}^{-3}$).[3] Moreover, ΔE (>70 meV) is large, indicating that the IB is isolated from the CB. The combination of small N_d and large ΔE allows us to treat the system as a non-degenerate system.[31]

The analysis presented above has two shortcomings. First, as can be seen in Table I that N_d accounts at most for 10% of the S dopants determined from the SIMS measurement. Similar experiments have also reported that more than 90% of the S dopants in hyperdoped Si are not electrically active as electron donors.[33,34] Second, we cannot obtain a good fit for the sample with the lowest dopant concentration (Sample A), because n_s is smaller at low temperatures, whereas the two-band model implies that n_H is at maximum at low temperature when all the carriers are in the IB (Eq. (1)). These discrepancies could be due to additional isolated energy levels.[35] Another possibility is that the inhomogeneous dopant concentration as a function of depth causes a partial freeze out of the carriers. Both the presence of additional isolated energy levels that are not electrically active and a variation in dopant concentration could cause the measured value of the carrier concentration to be lower than the dopant concentration.

Below the insulator-to-metal transition, the electron wave functions in the IB are localized, and carriers in the IB contribute to the conductivity by hopping from occupied states to empty states.[13] Because an activation energy is associated with carrier hopping, the conductivity decreases as temperature decreases. By fitting the measured conductivity data below 25 K to an Arrhenius equation, we obtain an activation energy of 0.53 ± 0.04 meV, consistent with hopping. Carrier hopping requires the presence of empty states or compensating acceptors (N_a).[36] When compensating acceptors are present, electrons occupy the compensating states, leaving behind empty states in the IB and enabling carriers in the IB to conduct by hopping from occupied states to empty states. While the presence of an activation energy supports hopping conduction, we do not know the origin of the compensating acceptors. In addition to the boron acceptors in the Si substrate, compensating acceptors could also be created during the hyperdoping or annealing process.[21]

The presence of a localized IB in samples where the sub-bandgap absorption is reduced by annealing (Figure 1(a)) implies that a localized IB does not necessarily give rise to sub-bandgap absorption. Consistent with our two-band model result, a narrow IB 70 meV below the CB is likely too shallow and narrow to contribute to broadband light absorption. Currently, annealing is necessary for carrying out Hall measurements and for the fabrication of devices, but we do not know how the band structure changes during annealing. Samples without the annealing treatment exhibit significant sub-bandgap absorption, so it will therefore be important to study the electronic properties of hyperdoped silicon before annealing. To this end one needs to reduce the laser irradiation damage so as to obviate the need for annealing.

We fabricate S-hyperdoped Si using femtosecond-laser hyperdoping at different SF_6 pressures. Our study shows that a localized IB does not necessarily give rise to sub-bandgap absorption. After furnace annealing, the sub-bandgap light absorption is significantly reduced, but the dopant concentration is sufficient to form a localized IB below the insulator-to-metal transition. Analyzing the temperature-dependent electronic transport data, we find that at the highest dopant concentration ($1.3 \times 10^{19}\,\mathrm{cm}^{-3}$), the IB is 70 meV below the CB minimum. This letter demonstrates how to extract a deep level IB location from a transport measurement, and the two-band model should be useful for analyzing IB energetics in other material systems for bulk IB devices, including photovoltaics.

The authors wish to acknowledge Dr. Mark Winkler, Dr. Christie Simmons, Dr. Joseph Sullivan, Professor Jacob Krich, and Professor Mike Aziz for valuable discussions. The authors also wish to acknowledge Benjamin Franta, Sarah Griesse-Nascimento, and Dr. Jin Suntivich for their assistance with editing the manuscript. The research described in this paper was supported by The National Science Foundation under Contract No. DMR-0934480. This work was performed in part at the Center for Nanoscale Systems (CNS), a member of the National Nanotechnology Infrastructure Network (NNIN), which is supported by the National Science Foundation under NSF Award No. ECS-0335765.

[1]C. Wu, C. H. Crouch, L. Zhao, J. E. Carey, R. Younkin, J. A. Levinson, E. Mazur, R. M. Farrell, P. Gothoskar, and A. Karger, Appl. Phys. Lett. **78**, 1850 (2001).
[2]S. H. Pan, D. Recht, S. Charnvanichborikarn, J. S. Williams, and M. J. Aziz, Appl. Phys. Lett. **98**, 121913 (2011).
[3]M. T. Winkler, D. Recht, M.-J. Sher, A. J. Said, E. Mazur, and M. J. Aziz, Phys. Rev. Lett. **106**, 178701 (2011).
[4]J. E. Carey, C. H. Crouch, M. Y. Shen, and E. Mazur, Opt. Lett. **30**, 1773 (2005).
[5]S. X. Hu, P. D. Han, S. Wang, X. Mao, X. Y. Li, and L. P. Gao, Semicond. Sci. Technol. **27**, 102002 (2012).
[6]K.-M. Guenther, T. Gimpel, J. W. Tomm, S. Winter, A. Ruibys, S. Kontermann, and W. Schade, Appl. Phys. Lett. **104**, 042107 (2014).
[7]E. Ertekin, M. T. Winkler, D. Recht, A. J. Said, M. J. Aziz, T. Buonassisi, and J. C. Grossman, Phys. Rev. Lett. **108**, 026401 (2012).
[8]In the context of this work, impurity band and the intermediate band have the same meaning, and we use these two terms interchangeably to be consistent with the literature we reference.
[9]C. S. Hung and J. R. Gliessman, Phys. Rev. **96**, 1226 (1954).
[10]C. Yamanouchi, K. Mizuguchi, and W. Sasaki, J. Phys. Soc. Jpn. **22**, 859 (1967).
[11]J. Basinski and R. Olivier, Can. J. Phys. **45**, 119 (1967).
[12]R. Ray and H. Fan, Phys. Rev. **121**, 768 (1961).
[13]N. F. Mott and W. D. Twose, Adv. Phys. **10**, 107 (1961).
[14]O. V. Emelyanenko, T. S. Lagunova, D. N. Nasledov, and G. N. Talalakin, Sov. Phys.-Solid State **7**, 1063 (1965).
[15]H. Neumann, Cryst. Res. Technol. **23**, 1377 (1988).
[16]A. Luque and A. Marti, Adv. Mater. **22**, 160 (2010).

This article is copyrighted as indicated in the article. Reuse of AIP content is subject to the terms at: http://scitation.aip.org/termsconditions.

[17] J. T. Sullivan, "Understanding the viability of impurity-band photovoltaics: A case study of S-doped Si," Ph.D. dissertation (Massachusetts Institute of Technology, 2013).
[18] E. Janzen, R. Stedman, G. Grossmann, and H. G. Grimmeiss, Phys. Rev. B **29**, 1907 (1984).
[19] T. F. Lee, R. D. Pashley, T. C. McGill, and J. W. Mayer, J. Appl. Phys. **46**, 381 (1975).
[20] V. V. Abramov, N. B. Brandt, V. A. Kulbachinskii, A. B. Timofeev, A. G. Ulyashin, N. V. Shlopak, and I. G. Gorolchuk, Sov. Phys. Semiconductors-USSR **25**, 310 (1991).
[21] V. A. Kulbachinskii, V. G. Kytin, V. V. Abramov, A. B. Timofeev, A. G. Ulyashin, and N. V. Shlopak, Sov. Phys. Semiconductors-USSR **26**, 1009 (1992).
[22] J. J. Krich, B. I. Halperin, and A. Aspuru-Guzik, J. Appl. Phys. **112**, 013707 (2012).
[23] J. T. Sullivan, R. G. Wilks, M. T. Winkler, L. Weinhardt, D. Recht, A. J. Said, B. K. Newman, Y. Zhang, M. Blum, S. Krause, W. L. Yang, C. Heske, M. J. Aziz, M. Bär, and T. Buonassisi, Appl. Phys. Lett. **99**, 142102 (2011).
[24] J. Olea, G. Gonzalez-Diaz, D. Pastor, I. Martil, A. Marti, E. Antolin, and A. Luque, J. Appl. Phys. **109**, 063718 (2011).
[25] P. Saring, A. Lena Baumann, B. Schlieper-Ludewig, S. Kontermann, W. Schade, and M. Seibt, Appl. Phys. Lett. **103**, 061904 (2013).
[26] M.-J. Sher, M. T. Winkler, and E. Mazur, MRS Bull. **36**, 439 (2011).
[27] W. Kern, *Handbook of Semiconductor Wafer Cleaning Technology: Science, Technology and Applications* (Noyes Publications, New Jersey, 1993).
[28] M.-J. Sher, "Intermediate band properties of femtosecond-laser hyperdoped silicon," Ph.D. dissertation (Harvard University, 2013).
[29] L. J. van der Pauw, Philips Tech. Rev. **20**, 220 (1958).
[30] S. M. Sze, *Physics of Semiconductor Devices* (Wiley-Interscience, New York, 1981), pp. 21 and 34.
[31] J. Blakemore, *Semiconductor Statistics* (Pergamon Press, New York, 1962), pp. 121–130 and 153–159.
[32] R. A. Smith, *Semiconductors* (Cambridge University Press, Cambridge, UK, 1978).
[33] M. Winkler, "Non-equilibrium chalcogen concentrations in silicon: Physical structure, electronic transport, and photovoltaic potential," Ph.D. dissertation (Harvard University, 2009).
[34] K.-M. Guenther, T. Gimpel, S. Kontermann, and W. Schade, Appl. Phys. Lett. **102**, 202104 (2013).
[35] B. I. Shklovskii and A. L. Efros, *Electronic Properties of Doped Semiconductors*, Springer Series in Solid-State Sciences Vol. 45 (Springer-Verlag, Berlin, 1984), pp. 25–36 and 76–82.
[36] E. M. Conwell, Phys. Rev. **103**, 51 (1956).

This article is copyrighted as indicated in the article. Reuse of AIP content is subject to the terms at: http://scitation.aip.org/termsconditions.